

Anisotropic nematic fluctuations above the ferroquadrupolar transition in TmVO_4

Z. Wang,¹ I. Vinograd¹,, Z. Mei,¹ P. Menegasso²,, D. Garcia,¹ P. Massat³,, I. R. Fisher,³ and N. J. Curro¹

¹*Department of Physics, University of California, Davis, California 95616, USA*

²*Instituto de Física “Gleb Wataghin,” UNICAMP, Campinas-SP 13083-859, Brazil*

³*Geballe Laboratory for Advanced Materials and Department of Applied Physics, Stanford University, California 94305, USA*



(Received 23 August 2021; revised 10 November 2021; accepted 10 November 2021; published 29 November 2021)

Ferroquadrupole order of local atomic orbitals provides a specific realization of electronic nematic order. TmVO_4 is an insulator and undergoes ferroquadrupolar order associated with the local Tm $4f$ orbitals at $T_Q = 2.15$ K. The material is a model system to study nematic order and the roles played by nematic fluctuations. Here we present ^{51}V nuclear magnetic resonance data as a function of field orientation in a single crystal. Although the spectra are well understood in terms of direct dipolar hyperfine couplings, the spin-lattice relaxation rate exhibits strong anisotropy that cannot be understood in terms of magnetic fluctuations. We find that the spin-lattice relaxation rate scales with the shear elastic constant associated with the ferroquadrupole phase transition, suggesting that quadrupole (nematic) fluctuations dominate the spin-lattice relaxation for in-plane fields.

DOI: [10.1103/PhysRevB.104.205137](https://doi.org/10.1103/PhysRevB.104.205137)

I. INTRODUCTION

Electronic nematic order refers to spontaneous breaking of discrete rotational symmetry in a crystal lattice by low energy electronic degrees of freedom, without further breaking translational symmetry. Bilinear coupling to lattice strain with the same symmetry necessarily leads to an accompanying lattice deformation. For the specific case corresponding to a tetragonal-to-orthorhombic phase transition, the nematic order parameter is an Ising variable, and hence in the absence of a symmetry-breaking field, domains with both possible orientations of the nematic director can be anticipated, each with a local C_2 symmetry but oriented at 90 degrees with respect to each other. Nematicity and nematic correlations may play a role in the low-temperature behavior of a number of strongly correlated electron systems, including the iron-based superconductors [1,2] and the high-temperature superconducting cuprates [3–5]. The correlation between large values of the nematic susceptibility, a putative nematic quantum critical point, and optimal superconductivity in several materials, point to a possible role for nematic fluctuations in the pairing interaction, as well as non-Fermi-liquid behavior in the normal state [6–9]. Disentangling the effects of nematicity can be complicated by the presence of other intertwined order parameters in such systems. It is challenging to discern whether nematic or antiferromagnetic fluctuations dominate, especially in a conducting system [10]. Moreover, since nematic order couples bilinearly to elastic strain with the same symmetry, the local strains that are associated with quenched random disorder, for example due to chemical substitution and other crystal defects, act as a random field for the nematic, and may give rise to inhomogeneous glassy behavior [11,12]. It is therefore important to investigate critical fluctuations in an Ising nematic system in the absence of metallicity or inhomogeneous strain fields.

Ferroquadrupole order of local atomic orbitals breaks only point symmetries and is a realization of nematic order. Such a phase transition requires local atomic states with either a non-Kramers or pseudo-Kramers degeneracy. Several rare-earth ions in suitable point symmetries meet this criterion and have the specific advantage that the underlying effective Hamiltonian is very well understood. The specific material studied here has the additional advantage that the crystal-field ground state, which is a non-Kramers doublet, is well-separated in energy from excited crystal-field levels. Hence, an elegant pseudospin representation can be used to describe the system, at least in weak fields, making this a model material system to study the effects of nematic fluctuations in insulators [13].

TmVO_4 is an insulator with Tm ions in the $4f^{12}$ configuration ($L = 5$, $S = 1$, $J = 6$) that crystallizes in space group $I41/amd$ (see inset of Fig. 1). The tetragonal crystal field splits the $J = 6$ multiplet, giving rise to a Γ_5 ground-state doublet separated by a gap of ≈ 77 K to the lowest excited state [14,15]. The wave functions of the ground state doublet are $|\psi_{1,2}\rangle = e|\pm 5\rangle + f|\pm 1\rangle + g|\mp 3\rangle$ in the J_z basis, where $e \approx 0.92$, $f \approx -0.37$, and $g \approx 0.12$. The degeneracy of these ground states cannot be lifted by a magnetic field perpendicular to the z direction because $\langle \psi_{1,2} | J_{\pm} | \psi_{1,2} \rangle = 0$, hence these form a non-Kramers doublet. The doublet can, however, be linearly split by either a magnetic field oriented along the c axis, or by lattice strains with either a B_{1g} ($x^2 - y^2$) or B_{2g} (xy) symmetry. Quadrupole-quadrupole interactions mediated by the lattice dominate the magnetic interactions, and the material undergoes a cooperative Jahn-Teller ferroquadrupolar ordering with a B_{2g} symmetry at $T_Q = 2.15$ K, accompanied by an orthorhombic lattice distortion of the same symmetry [16]. The low-temperature behavior of the Tm quadrupoles can be well described by the transverse field Ising model, in which pseudospins ($\tilde{S} = 1/2$) experience in-plane ferroquadrupolar Ising couplings and couple to a transverse

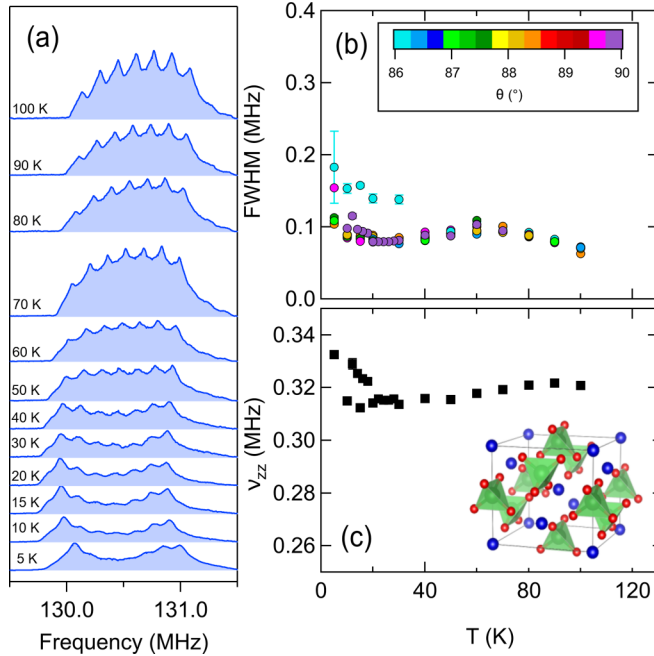


FIG. 1. (a) ^{51}V spectra in TmVO_4 at 11.7294 T for $\mathbf{H}_0 \perp c$ at several different temperatures. The (b) full-width half maximum and (c) quadrupolar splitting versus temperature for several different angles θ . The inset shows the unit-cell structure. Tm is blue, V is green (within the pyramids), and O is red.

magnetic field along the z axis [17]. These fields will enhance the fluctuations of the pseudospins and can tune the system to an Ising-nematic quantum phase transition. This material thus offers an important platform to investigate quantum critical nematic fluctuations in an insulator.

To better understand the nature of these fluctuations we have investigated ^{51}V ($I = 7/2$, $Q = 52$ mb, 99.75% abundant) NMR in a single crystal of TmVO_4 in a magnetic field $\mathbf{H}_0 = 11.72$ T oriented perpendicular to the c axis. We find that the magnetic shift and spin-lattice relaxation rate are strongly angular dependent (rotating the field in the a - c plane) below ≈ 80 K, reflecting the anisotropy of the ground-state doublet. The spin-lattice relaxation rate is nonmonotonic, exhibiting a large enhancement at low temperature that may be associated with critical nematic fluctuations. The spectrum exhibits a strong temperature-dependent magnetic linewidth broadening at low temperatures caused by inhomogeneous magnetic demagnetization fields.

II. NMR SPECTRA AND MAGNETIC SHIFT

TmVO_4 crystals were grown from a $\text{Pb}_2\text{V}_2\text{O}_7$ flux using 4 mole percent of Tm_2O_3 , following the methods described in Refs. [18,19]. The crystals have a rod-like morphology with the c axis along the long axis. A single crystal of approximate dimension 1 mm \times 1 mm \times 4 mm was selected and mounted on a cryogenic NMR probe equipped with a mechanical goniometer [20]. The magnetic susceptibility is strongly anisotropic, reflecting that of the unusual g factor ($g_c \approx 10.2$, $g_{\perp} = 0$) of the ground-state doublet. Although a crystal mounted with $c \perp \mathbf{H}_0$ experiences zero torque, it is an

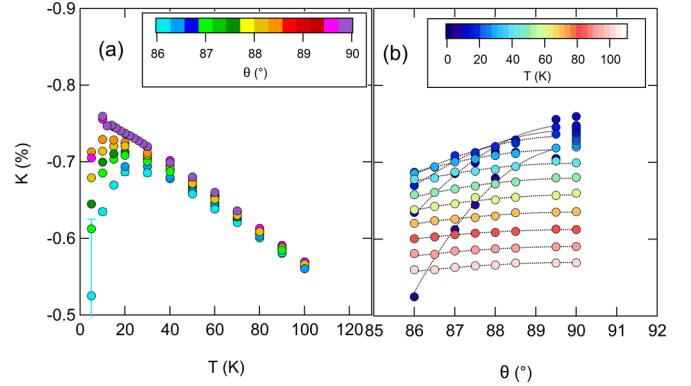


FIG. 2. Magnetic shift K versus (a) temperature and (b) angle. The dotted lines are fits as described in the text.

unstable equilibrium and there is a large torque for infinitesimal deviations from 90° . To alleviate this issue we secured the crystal with epoxy to a mounting plate that itself is rotated. Spin echoes were acquired at several different frequencies, and the Fourier transforms were summed to measure the full spectra including all nuclear-spin transitions. Figure 1(a) shows several representative spectra of the ^{51}V as a function of temperature. There are seven peaks separated by the quadrupolar interaction. Because the V has axial symmetry, the peaks frequencies are given by

$$\nu = \gamma H_0 [1 + K(\theta)] + n\nu_q(\theta), \quad (1)$$

where the magnetic, $K(\theta)$, and quadrupolar, $\nu_q(\theta)$, shifts vary with the angle θ between the c axis and \mathbf{H}_0 :

$$K(\theta) = K_{cc} \cos^2 \theta + K_{aa} \sin^2 \theta, \quad (2)$$

$$\nu_q(\theta) = \nu_{zz}(3 \cos^2 \theta - 1)/2. \quad (3)$$

Here $\gamma = 11.193$ MHz/T, $n = -3, \dots, 3$, $\nu_{zz} = eQV_{zz}/12h$, and V_{zz} is the electric-field gradient at the V site. We measured the spectra for several angles $86^\circ \leq \theta \leq 90^\circ$ and fit the spectra to a sum of Lorentzians. The temperature and angular dependence of the linewidths, EFG, and magnetic shifts are shown in Figs. 1(b), 1(c), and 2(a).

We find that the EFG is similar to previous measurements [14,21]; however, the linewidths are broad. For this orientation, the quadrupolar splitting is $\nu_{zz}/2$, which is comparable to the full width at half maximum (FWHM) of each resonance. As a result, the individual peaks become difficult to resolve at low temperatures. Each of the satellite resonances has the same linewidth, implying that the broadening is due to magnetic field inhomogeneity within the sample. Moreover, we find that the spectra are narrower at lower applied fields and that the FWHM varies approximately linearly with field. Since the susceptibility is strongly anisotropic, distortions of the internal field \mathbf{B} due to demagnetization effects within the needle-like prism of the crystal can create a large distribution of local resonance frequencies [22]. The spectra also display a suppression of intensity for the inner satellites, particularly at low temperature. This phenomenon arises due to fast spin-spin decoherence rates (T_2^{-1}) with high spin nuclei [23,24].

The magnetic shift shown in Fig. 2 is negative and strongly angular dependent at low temperature. We fit the angular

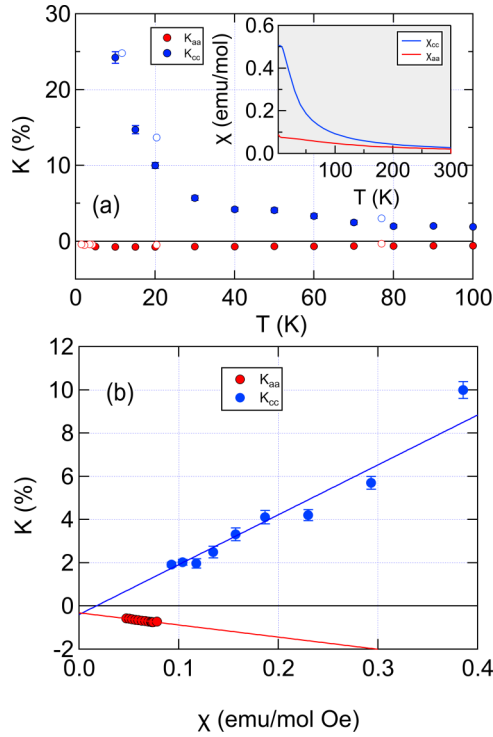


FIG. 3. K_{aa} and K_{cc} versus (a) temperature and (b) bulk susceptibility. The open points correspond to values reported in Ref. [14]. The solid lines are fits as described in the text. The inset displays the bulk susceptibility versus temperature.

dependence to extract the tensor components K_{aa} and K_{cc} , shown as dotted lines in Fig. 2(b). This approach enables us to extract the magnetic shift for the c direction without needing to fully align the crystal in this orientation, although the error bars for K_{cc} are larger than for K_{aa} . The temperature dependence of K_{aa} and K_{cc} is shown in Fig. 3(a). K_{cc} is large and positive. Figure 3(b) shows these shift components plotted versus the bulk susceptibility $\chi_{aa,cc}$, which was measured independently by using a SQUID magnetometer. The shift varies linearly with susceptibility as $K_{\alpha\alpha} = K_{\alpha\alpha}^{\text{orb}} + A_{\alpha\alpha}\chi_{\alpha\alpha}$, where $A_{\alpha\beta}$ are the components of the hyperfine coupling tensor. We find that $K_{aa}^{\text{orb}} = -0.315 \pm 0.009\%$, $K_{cc}^{\text{orb}} = -0.4 \pm 0.1\%$, $A_{aa} = -0.32 \pm 0.07$ kOe/ μ_B , and $A_{cc} = 1.29 \pm 0.05$ kOe/ μ_B .

These values of the hyperfine couplings are consistent with a direct dipolar coupling mechanism between the Tm moments and the V nuclear spins. The direct dipolar coupling is given by $A_{\alpha\beta}^{\text{dip}} = \sum_i (\nabla \times \mathbf{A}_i)_{\alpha/\mu\beta}$, where $\mathbf{A}_i = \boldsymbol{\mu} \times \mathbf{r}_i/r_i^3$ is the vector potential of a dipole moment $\boldsymbol{\mu}$ located at lattice site \mathbf{r}_i relative to a central nucleus. For the TmVO₄ lattice, we estimate $A_{aa}^{\text{dip}} = A_{bb}^{\text{dip}} = -0.336$ kOe/ μ_B and $A_{cc}^{\text{dip}} = 0.671$ kOe/ μ_B at the V site. The theoretical value for the perpendicular direction is the same as the measured value within the error limits. For the c axis, the theoretical value is within a factor of two of the measured values, and it is likely that there are larger systematic measurement errors involved in extracting this value. Thus the anisotropic magnetic shift tensor can be fully explained via direct dipolar interactions, as expected for an insulator.

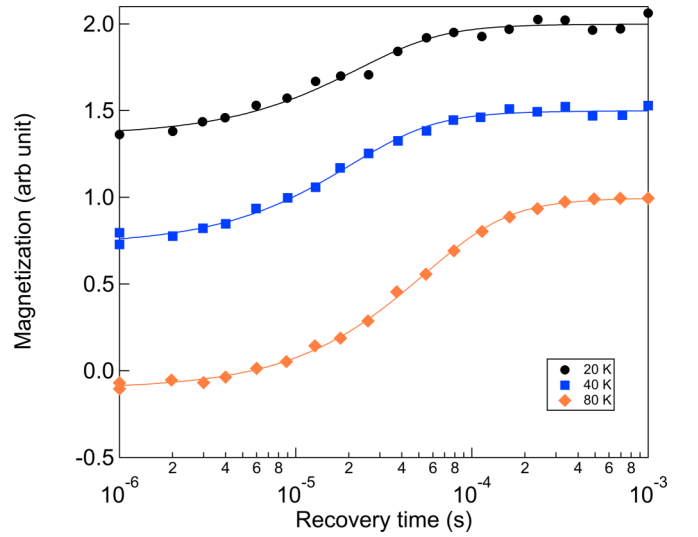


FIG. 4. Magnetization recovery curves at 20, 40, and 80 K for $\theta = 88^\circ$. Solid lines are fits as described in the text. The data have been normalized and offset vertically for clarity.

III. SPIN-LATTICE RELAXATION RATE

The spin-lattice relaxation rate T_1^{-1} was measured by applying initialization pulses at the central transition ($n = 0$) and measuring the echo intensity as a function of recovery time using low power pulses with small bandwidths (pulse widths 6–8 μs), repetition time 10 ms, pulse spacing 20 μs , and pulse power of 39–44 dBm. Representative recovery curves are displayed in Fig. 4. The magnetization recovery was fit to the standard expression for magnetic fluctuations: $M(t) = M_0[1 - 2f\phi(t/T_1)]$, where M_0 is the equilibrium magnetization, f is the inversion fraction, and

$$\phi(t) = \frac{1225}{1716}e^{-28t} + \frac{75}{364}e^{-15t} + \frac{3}{44}e^{-6t} + \frac{1}{84}e^{-t}. \quad (4)$$

This expression fits the data well without the need for a stretching exponent, but the fraction f is reduced at lower temperatures due to the inhomogeneous magnetic broadening. Figure 5 shows the temperature and angular dependence of T_1^{-1} . For $\theta = 90^\circ$, T_1^{-1} decreases strongly below 80 K as the excited crystal-field levels are thermally depopulated. In this temperature range, T_1^{-1} becomes strongly angular dependent, increasing by more than a factor of 30 as the field \mathbf{H}_0 rotates by only 4° away from the perpendicular configuration, and the spin-spin relaxation time T_2 grows shorter, to less than 100 μs . This behavior likely reflects the anisotropy of the g factor of the ground-state doublet, however, the anisotropy of T_1^{-1} is puzzling. If the relaxation is driven by magnetic fluctuations of the Tm ground state, then T_1^{-1} should exhibit a *maximum* at $\theta = 90^\circ$ rather than a minimum because fluctuations of the non-Kramers doublet should lie exclusively along the c axis. Therefore $T_1^{-1}(0^\circ)$ should be much smaller than $T_1^{-1}(90^\circ)$, in contrast with our observations.

A. Magnetic fluctuations

On the other hand, the hyperfine couplings can give rise to a more complicated relationship between the direction of

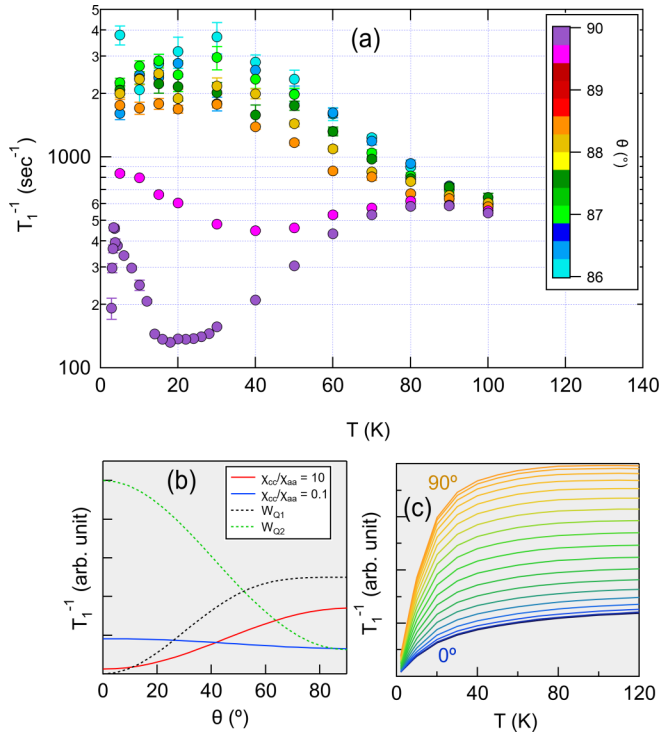


FIG. 5. (a) T_1^{-1} vs temperature for multiple angles. (b) Calculated T_1^{-1} versus θ for magnetic fluctuations (solid lines) and for quadrupole fluctuations (dashed lines). (c) Calculated T_1^{-1} versus temperature and angle using Eq. (5), where the angle is increased in 5° increments between 0° and 90° .

the Tm moments and the direction of the hyperfine fields. To properly account for these couplings we use the Moriya expression:

$$T_{1m}^{-1} = \gamma^2 k_B T \lim_{\omega \rightarrow 0} \sum_{\mathbf{q}, \alpha, \beta} \mathcal{F}_{\alpha\beta}(\mathbf{q}) \frac{\text{Im} \chi_{\alpha\beta}(\mathbf{q}, \omega)}{\hbar \omega}, \quad (5)$$

where the form factors $\mathcal{F}_{\alpha\beta}(\mathbf{q})$ (see Appendix A for details) depend on the local dipolar hyperfine couplings, and $\chi_{\alpha\beta}(\mathbf{q}, \omega)$ is the dynamical magnetic susceptibility of the Tm moments. For simplicity we only include the two nearest-neighbor and four next-nearest-neighbor Tm atoms in the form factors. Because the Tm system exhibits ferroquadrupolar order at T_Q , we assume that the structure of the dynamical susceptibility can be modeled as

$$\chi_{\alpha\alpha}(\mathbf{q}, \omega) = \frac{\chi_{\alpha\alpha}(T)}{\xi^{-2} + f(\mathbf{q}) - i\omega/\Gamma q}, \quad (6)$$

where ξ is a correlation length, Γ is a characteristic fluctuation energy, $f(\mathbf{q}) = q_x^2 + q_y^2 + \eta q_z^2$, η is a dimensionless parameter that reflects the tetragonal nature, and $\chi_{\alpha\alpha}(T)$ is the static ($\mathbf{q} = 0$) susceptibility. ξ and η are unknown parameters, but we compute the temperature and angular dependence using $\xi = 2$ and $\eta = 1/2$. Figure 5(b) shows the expected angular dependence of T_{1m}^{-1} for $\chi_{cc}/\chi_{aa} = 10$ (red), close to the experimental value, and for $\chi_{cc}/\chi_{aa} = 0.1$ (blue). The former clearly exhibits a maximum of T_{1m}^{-1} at $\theta = 90^\circ$, in contrast with our observations. The latter exhibits a shallow minimum at 90° , but the susceptibility anisotropy does not agree with

experiment. Figure 5(c) shows the temperature dependence using the measured values of the static susceptibility. Although there is an overall decrease in T_{1m}^{-1} at lower temperatures, the detailed temperature dependence does not match experiment, and the calculated T_1^{-1} still exhibits a maximum for $\theta = 90^\circ$ at all temperatures. Despite the complex form factors for the direct dipolar couplings, the expected magnetic fluctuations of the Tm ground state cannot explain the observed increase in T_1^{-1} as the field rotates out of the plane. Moreover, we have checked a model for the dynamical susceptibility with antiferromagnet fluctuations that peaks at a finite wave vector \mathbf{q} and find that the expected anisotropy of T_1^{-1} does not match our observations.

B. Quadrupolar fluctuations

An alternative explanation is that the spin-lattice relaxation rate is dominated by quadrupolar fluctuations rather than magnetic. The Tm quadrupole moments couple to the EFG at the V site, giving rise to a second nuclear quadrupolar relaxation channel [10]. The enhancement of T_1^{-1} below 20 K for $\theta = 90^\circ$ may represent the growth of critical fluctuations near T_Q . Note that changing θ by only 0.25° dramatically alters T_1^{-1} , which is close to the limit of precision of our goniometer. Thus it is possible that the enhancement below 20 K may vanish or become smaller for better alignment. In the presence of both magnetic and quadrupolar relaxation, the expression for $\phi(t)$ [Eq. (4)] changes and includes three independent rates: T_{1m}^{-1} , W_{Q1} , and W_{Q2} , where the latter two are associated with $\Delta m = \pm 1$ and $\Delta m = \pm 2$ quadrupolar relaxation. We are unable, however, to independently extract these parameters with sufficient resolution. Moreover, the line broadening observed in Fig. 1 also means that the magnetization relaxation at the central transition may also include contributions from nearby satellite transitions, further complicating any attempts to extract the independent relaxation channels. Nevertheless, it is instructive to consider the case where quadrupole fluctuations dominate and magnetic fluctuations can be neglected.

For a tetragonal-to-orthorhombic distortion, quadrupolar relaxation is driven by fluctuations of the spherical tensor components of the EFG: $V_{\pm 1} = V_{zx} \pm iV_{zy}$ and $V_{\pm 2} = \frac{1}{2}(V_{xx} - V_{yy}) \pm iV_{xy}$, where the $V_{\alpha\beta}$ are the EFG tensor components relative to the direction of \mathbf{H}_0 . These give rise to nuclear-spin relaxation rates:

$$W_{Q1, Q2} = (eQ/\hbar)^2 \int_0^\infty \langle V_{+1,2}(\tau) V_{-1,2}(0) \rangle e^{-\omega_L \tau} d\tau, \quad (7)$$

where ω_L is the Larmor frequency [25]. The ferroquadrupolar order in this system has B_{2g} symmetry, so $V_{xx} - V_{yy} \neq 0$, where z corresponds to the c direction and x and y are along the principal axes of the EFG tensor, which are rotated 45° relative to the tetragonal a axes. Above T_Q fluctuations of $V_{\pm 2}$ should dominate those of $V_{\pm 1}$, and as a result we anticipate that $W_{Q1}(\theta = 0)$ can be neglected. As the field is rotated towards the plane, the EFG tensor components change, and the relaxation rates become angular dependent (see Appendix B for details):

$$W_{Q2}(\theta)/W_{Q2}(0) = (\cos^4 \theta + 6 \cos^2 \theta + 1)/8, \quad (8)$$

$$W_{Q1}(\theta)/W_{Q2}(0) = \sin^2 \theta [\cos(2\theta) + 3]/4. \quad (9)$$

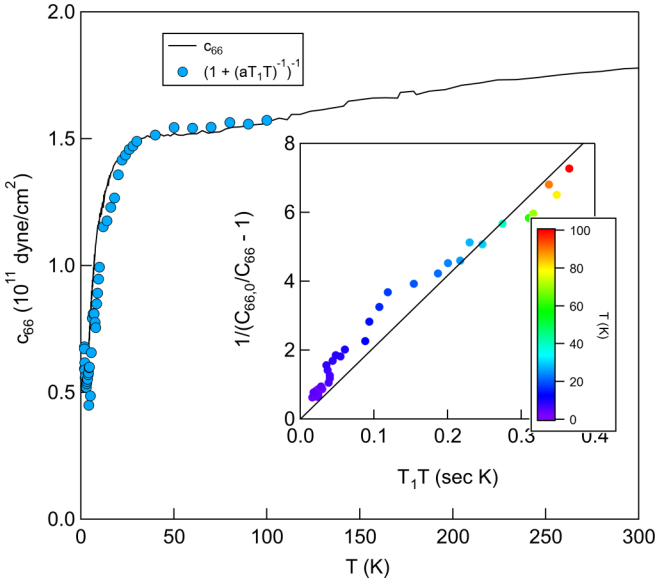


FIG. 6. The shear elastic stiffness coefficient c_{66} (solid line, reproduced from Ref. [26]) and the quantity $1/[1 + (aT_1T)^{-1}]$ as a function of temperature. Inset shows $1/(c_{66,0}/c_{66} - 1)$ versus T_1T , with temperature implicit. The solid black line is the best linear fit, giving $a = 18.5 \pm 0.4 \text{ s}^{-1} \text{ K}^{-1}$.

These quantities are shown in Fig. 5(b) as dashed lines. W_{Q2} exhibits a minimum for $\theta = 90^\circ$, whereas W_{Q1} is nearly independent of θ at this angle. This behavior agrees qualitatively with our observations, but the increases we observe are in fact a much stronger function of angle than expected for quadrupolar relaxation. Rotating θ by 1° – 2° out of the plane enhances T_1^{-1} by an order of magnitude, whereas W_{Q2} exhibits only a quadratic minimum at this angle.

The interpretation that relaxation is driven by quadrupole fluctuations is supported by comparisons of the temperature dependence of T_1^{-1} with that of the shear elastic stiffness coefficient c_{66} , which softens with decreasing temperature and vanishes at T_Q [26]. This behavior is driven by the nematic susceptibility: $\chi_{nem} = c_{66,0}(1 - c_{66,0}/c_{66})/\lambda^2$, where λ is the coupling between the lattice and the Tm $4f$ orbitals, and $c_{66,0}$ is the stiffness coefficient in the absence of the coupling [27]. If T_1^{-1} is also determined by the Tm orbital fluctuations, then $(T_1T)^{-1} \sim \chi_{nem}$ (see Appendix C for details) [10,28,29]. We thus expect $T_1T \sim (c_{66,0}/c_{66} - 1)^{-1}$, which is demonstrated in Fig. 6. The main panel compares the temperature dependence of c_{66} with the measured T_1^{-1} values, and the inset shows the scaling between the shear modulus and T_1^{-1} with temperature as an implicit parameter. The scaling in Fig. 6 suggests that the spin-lattice relaxation is driven primarily by quadrupole fluctuations, which are reflected in the softening of c_{66} . The temperature dependence of c_{66} also includes contributions from the higher CEF levels [26], which suggest that these also play a role in the spin-lattice relaxation rate at these temperatures. Note that the sharp drop in c_{66} below ≈ 30 K corresponds roughly with the increase in ν_{zz} observed in Fig. 1(c). It is possible that the softening of the lattice is reflected in changes to the static EFG as well.

IV. DISCUSSION

A slightly different scaling relationship was found in the iron pnictide superconductors via a microscopic model that assumes that the nematicity arises in the magnetic susceptibility, which in turn affects the nuclei through a magnetic hyperfine interaction [27]. In TmVO₄, the nematicity arises from the Tm electronic orbitals, and the coupling to the nuclei may be through the quadrupolar interaction. Moreover, the pnictide model assumed the presence of Landau damping by a Fermi surface of quasiparticles, which is not the case for insulating TmVO₄. The relaxation in TmVO₄ must also involve a damping term, but the origin of this term is unknown. The fact that the scaling relationship in Fig. 6 holds suggests that this damping term is temperature independent.

Rotating the field away from 90° can enhance quadrupole fluctuations. A rotation of \mathbf{H}_0 by 4° corresponds to a field of 0.82 T along the c axis. This is greater than the critical field of $H_c = 0.52$ T to suppress the long-range nematic order, which naturally enhances fluctuations of both $V_{\pm 2}$ and $V_{\pm 1}$. However, these critical fluctuations are not likely to persist to higher temperatures beyond $\approx 10T_Q$, and thus are unlikely to be responsible for the large anisotropy observed up to 80 K. An alternative scenario is that the higher CEF levels cannot be ignored. Indeed, even though the in-plane g factor of the non-Kramers doublet vanishes in zero applied field, the excited CEF levels can be mixed into the ground-state wave functions by an in-plane field. As a result, there can be an induced magnetic moment in the plane, which may also contribute to the relaxation [26].

It is likely that the spin-lattice relaxation is dominated by both magnetic and quadrupolar fluctuations, however it is difficult to disentangle these two relaxation channels without more detailed measurements of the relaxation at the higher satellite transitions [25]. However, as illustrated in Fig. 1, the satellites are magnetically broadened and cannot be well resolved, especially at lower temperatures. This broadening is due to the demagnetization field inhomogeneity of our crystal. In principle, it is possible to improve the spectral resolution by removing the sharp edges and corners of the sample and/or operating at lower applied fields, in order to better discern the individual satellite transitions.

Nuclear spin-lattice relaxation rates have also been studied in both PrAlO₃ and CsCuCl₃, materials that exhibit structural distortions due to the cooperative Jahn-Teller effect with nonmagnetic ground states [30–32]. In contrast with our observations in TmVO₄, T_1^{-1} did not exhibit any enhancement above the phase transition in these cases, even though the EFG changed below. On the other hand, unlike TmVO₄, the phase transitions in these cases are first order, thus T_1^{-1} should not reflect any critical slowing down. The spin-lattice relaxation rate in the disordered state was analyzed in terms of magnetic (hyperfine) fluctuations, although the nuclei in question (^{27}Al , $I = 5/2$ and ^{133}Cs , $I = 7/2$) are quadrupolar and should be sensitive to fluctuations of the EFG.

In summary, we have measured the spectra and relaxation rates in TmVO₄ as a function of temperature and field

TABLE I. Position vectors for six nearest-neighbor Tm sites to V, in spherical coordinates.

\mathbf{r}_i	r (Å)	θ (°)	ϕ (°)
1	3.13030	0	0
2	3.13030	180	0
3	3.86654	66.1218	0
4	3.86654	113.8782	90
5	3.86654	66.1218	180
6	3.86654	113.8782	270

direction oriented perpendicular to the c axis. We find that the magnetic shift tensor agrees quantitatively with direct dipolar coupling between the V nuclear moments and the Tm $4f$ moments. The spin-lattice relaxation rate exhibits a steep minimum for a field oriented 90° to the c axis, which

is inconsistent with purely magnetic fluctuations. We find that T_1 scales with the lattice constant for shear strain, c_{66} , which softens and vanishes at the nematic transition. It is likely that both quadrupolar and magnetic fluctuations are present and drive spin-lattice relaxation. However, the origin of the steep angular dependence of T_1^{-1} remains an open question.

ACKNOWLEDGMENTS

We acknowledge helpful discussions with R. Fernandes. Work at UC Davis was supported by the NSF under Grants No. DMR-1807889 and No. PHY-1852581, as well as the UC Davis Seed Grant program. Crystal growth performed at Stanford University was supported by the Air Force Office of Scientific Research under Award No. FA9550-20-1-0252. P.M. was partially supported by the Gordon and Betty Moore Foundation Emergent Phenomena in Quantum Systems Initiative through Grant No. GBMF9068.

APPENDIX A: MAGNETIC RELAXATION FORM FACTORS

We assume that the dominant hyperfine fields at the V site arise from the two nearest-neighbor and four next-nearest-neighbor Tm moments, whose positions are given in Table I. We define

$$\mathcal{A}_{\alpha\beta}(\mathbf{q}) = \sum_i e^{i\mathbf{q}\cdot\mathbf{r}_i} A_{\alpha\beta}^{\text{dip}}, \quad (\text{A1})$$

where $A_{\alpha\beta}^{\text{dip}}$ is defined in the main text. For an applied field \mathbf{H}_0 oriented at angles θ and ϕ relative to the crystalline axes, the form factors are [33]

$$\mathcal{F}_{\alpha\beta}(\mathbf{q}) = \sum_{\epsilon,\delta} [R_{x\epsilon}R_{x\delta} + R_{y\epsilon}R_{y\delta}] \mathcal{A}_{\epsilon\alpha}(\mathbf{q}) \mathcal{A}_{\delta\beta}(-\mathbf{q}), \quad (\text{A2})$$

where the $R_{\alpha\beta}$ are elements of the three-dimensional (3D) rotation matrix:

$$\mathbb{R} = \begin{pmatrix} \cos\theta \cos^2\phi + \sin^2\phi & \cos\theta \cos\phi \sin\phi - \cos\phi \sin\phi & \cos\phi \sin\theta \\ \cos\theta \cos\phi \sin\phi - \cos\phi \sin\phi & \cos^2\phi + \cos\theta \sin^2\phi & \sin\theta \sin\phi \\ -\cos\phi \sin\theta & -\sin\theta \sin\phi & \cos\theta \end{pmatrix}. \quad (\text{A3})$$

APPENDIX B: QUADRUPOLEAR RELAXATION ANISOTROPY

Equation (7) gives the expression for quadrupolar relaxation in terms of the spherical tensor components of the EFG tensor. The quadrupolar interaction is only on-site, so there are no form factors. However, the EFG tensor must be rotated properly as the field direction changes. Under a rotation the tensor operators $V_m(\tau)$ transform as

$$V'_m(\tau) = \sum_{m'} D_{mm'}^{(2)} V_{m'}(\tau), \quad (\text{B1})$$

where

$$D_{mm'}^{(l)}(\alpha, \beta, \gamma) = e^{-im\alpha} d_{mm'}^l(\beta) e^{-im'\gamma} \quad (\text{B2})$$

are the Wigner D matrices, $m, m' = -l, \dots, +l$, and the Euler angles are ($\alpha = \phi, \beta = \theta, \gamma = 0$). The correlation functions $\langle V_m(\tau) V_{-m}(0) \rangle$ are thus given by

$$\langle V'_m(\tau) V'_{-m}(0) \rangle = \sum_{m', m''} D_{2m'}^{(2)}(\phi, \theta) D_{-2m''}^{(2)}(\phi, \theta) \langle V_{m'}(\tau) V_{m''}(0) \rangle. \quad (\text{B3})$$

We assume that $\langle V_m(\tau) V_{m'}(0) \rangle = 0$ for all m, m' except for $m = -m' = 2$ and $m = m' = 1$. Moreover, we assume that $\langle V_2(\tau) V_{-2}(0) \rangle \gg \langle V_1(\tau) V_{-1}(0) \rangle$, since $\langle V_{\pm 2} \rangle \neq 0$ and $\langle V_{\pm 1} \rangle = 0$ in the nematic phase. We thus expect $W_{Q1}(\theta = 0) \approx 0$, and

$$W_{Q2}(\theta)/W_{Q2}(0) = (\cos^4\theta + 6\cos^2\theta + 1)/8, \quad (\text{B4})$$

$$W_{Q1}(\theta)/W_{Q2}(0) = \sin^2\theta [\cos(2\theta) + 3]/4, \quad (\text{B5})$$

as given in the main text in Eqs. (8) and (9).

APPENDIX C: RELAXATION DRIVEN BY NEMATIC FLUCTUATIONS

We note that Eq. (7) can be expressed in terms of the dynamical nematic susceptibility [10]:

$$W_{Q2}(0) = \left(\frac{eQ}{\hbar}\right)^2 k_B T \lim_{\omega \rightarrow 0} \sum_{\mathbf{q}} \frac{\text{Im} \chi_{nem}(\mathbf{q}, \omega)}{\hbar \omega}. \quad (\text{C1})$$

The dynamical susceptibility can be expressed phenomenologically as $\chi_{nem}(\mathbf{q}, \omega) = \chi_{nem}(1 - i\omega/\omega_n)^{-1}$, where χ_{nem} is the static nematic susceptibility and ω_n is a damping term [28,29]. In this case $W_{Q2}(0) = (eQ)^2 k_B T \chi_{nem}/\hbar^2 \omega_n$.

-
- [1] R. M. Fernandes, A. V. Chubukov, and J. Schmalian, What drives nematic order in iron-based superconductors? *Nat. Phys.* **10**, 97 (2014).
- [2] S.-H. Baek, D. V. Efremov, J. M. Ok, J. S. Kim, J. van den Brink, and B. Büchner, Orbital-driven nematicity in FeSe, *Nat. Mater.* **14**, 210 (2015).
- [3] S. A. Kivelson, E. Fradkin, and V. J. Emery, Electronic liquid-crystal phases of a doped Mott insulator, *Nature (London)* **393**, 550 (1998).
- [4] M. Vojta, Lattice symmetry breaking in cuprate superconductors: Stripes, nematics, and superconductivity, *Adv. Phys.* **58**, 699 (2009).
- [5] M. J. Lawler, K. Fujita, J. Lee, A. R. Schmidt, Y. Kohsaka, C. K. Kim, H. Eisaki, S. Uchida, J. C. Davis, J. P. Sethna, and E.-A. Kim, Intra-unit-cell electronic nematicity of the high- T_c copper-oxide pseudogap states, *Nature (London)* **466**, 347 (2010).
- [6] J.-H. Chu, H.-H. Kuo, J. G. Analytis, and I. R. Fisher, Divergent nematic susceptibility in an iron arsenide superconductor, *Science* **337**, 710 (2012).
- [7] H.-H. Kuo, J.-H. Chu, J. C. Palmstrom, S. A. Kivelson, and I. R. Fisher, Ubiquitous signatures of nematic quantum criticality in optimally doped Fe-based superconductors, *Science* **352**, 958 (2016).
- [8] S. Lederer, Y. Schattner, E. Berg, and S. A. Kivelson, Enhancement of Superconductivity Near a Nematic Quantum Critical Point, *Phys. Rev. Lett.* **114**, 097001 (2015).
- [9] T. A. Maier and D. J. Scalapino, Pairing interaction near a nematic quantum critical point of a three-band CuO_2 model, *Phys. Rev. B* **90**, 174510 (2014).
- [10] A. P. Dioguardi, T. Kissikov, C. H. Lin, K. R. Shirer, M. M. Lawson, H.-J. Grafe, J.-H. Chu, I. R. Fisher, R. M. Fernandes, and N. J. Curro, NMR Evidence for Inhomogeneous Nematic Fluctuations in $\text{BaFe}_2(\text{As}_{1-x}\text{P}_x)_2$, *Phys. Rev. Lett.* **116**, 107202 (2016).
- [11] A. P. Dioguardi, M. M. Lawson, B. T. Bush, J. Crocker, K. R. Shirer, D. M. Nisson, T. Kissikov, S. Ran, S. L. Bud'ko, P. C. Canfield, S. Yuan, P. L. Kuhns, A. P. Reyes, H.-J. Grafe, and N. J. Curro, NMR evidence for inhomogeneous glassy behavior driven by nematic fluctuations in iron arsenide superconductors, *Phys. Rev. B* **92**, 165116 (2015).
- [12] E. W. Carlson, K. A. Dahmen, E. Fradkin, and S. A. Kivelson, Hysteresis and Noise from Electronic Nematicity in High-Temperature Superconductors, *Phys. Rev. Lett.* **96**, 097003 (2006).
- [13] P. Massat, J. Wen, J. M. Jiang, A. T. Hristov, Y. Liu, R. S. Feigelson, Y. S. Lee, R. M. Fernandes, and I. R. Fisher, Field-tuned ferroquadrupolar quantum phase transition in the insulator TmVO_4 , [arXiv:2110.03791](https://arxiv.org/abs/2110.03791).
- [14] B. Bleaney and M. R. Wells, Radiofrequency studies of TmVO_4 , *Proc. R. Soc. London. Series A* **370**, 131 (1980).
- [15] G. J. Bowden, A review of the low temperature properties of the rare earth vanadates, *Aust. J. Phys.* **51**, 201 (1998).
- [16] G. A. Gehring and K. A. Gehring, Co-operative Jahn-Teller effects, *Rep. Prog. Phys.* **38**, 1 (1975).
- [17] A. V. Maharaj, E. W. Rosenberg, A. T. Hristov, E. Berg, R. M. Fernandes, I. R. Fisher, and S. A. Kivelson, Transverse fields to tune an Ising-nematic quantum phase transition, *Proc. Natl. Acad. Sci. USA* **114**, 13430 (2017).
- [18] R. Feigenson, Flux growth of type RVO_4 rare-earth vanadate crystals, *J. Am. Ceram. Soc.* **51**, 538 (1968).
- [19] S. Smith and B. Wanklyn, Flux growth of rare earth vanadates and phosphates, *J. Cryst. Growth* **21**, 23 (1974).
- [20] T. Shiroka, F. Casola, J. Mesot, W. Bachmann, and H.-R. Ott, A two-axis goniometer for low-temperature nuclear magnetic resonance measurements on single crystals, *Rev. Sci. Instrum.* **83**, 093901 (2012).
- [21] B. Bleaney, J. Gregg, A. de Oliveira, and M. Wells, Nuclear electric quadrupole interaction in LnVO_4 , *J. Magn. Magn. Mater.* **31-34**, 745 (1983).
- [22] M. Lawson, B. T. Bush, T. Kissikov, Z. Brubaker, K. R. Shirer, J. R. Jeffries, S. Ran, I. Jeon, M. B. Maple, and N. J. Curro, Measurements of the NMR Knight shift tensor and nonlinear magnetization in URu_2Si_2 , *Phys. Rev. B* **97**, 075138 (2018).
- [23] D. M. Nisson, A. P. Dioguardi, P. Klavins, C. H. Lin, K. Shirer, A. C. Shockley, J. Crocker, and N. J. Curro, Nuclear magnetic resonance as a probe of electronic states of Bi_2Se_3 , *Phys. Rev. B* **87**, 195202 (2013).
- [24] B.-L. Young, Z.-Y. Lai, Z. Xu, A. Yang, G. D. Gu, Z.-H. Pan, T. Valla, G. J. Shu, R. Sankar, and F. C. Chou, Probing the bulk electronic states of Bi_2Se_3 using nuclear magnetic resonance, *Phys. Rev. B* **86**, 075137 (2012).
- [25] A. Suter, M. Mali, J. Roos, and D. Brinkmann, Mixed magnetic and quadrupolar relaxation in the presence of a dominant static Zeeman Hamiltonian, *J. Phys.: Condens. Matter* **10**, 5977 (1998).
- [26] R. L. Melcher, E. Pytte, and B. A. Scott, Phonon Instabilities in TmVO_4 , *Phys. Rev. Lett.* **31**, 307 (1973).

- [27] R. M. Fernandes, A. E. Böhrer, C. Meingast, and J. Schmalian, Scaling between Magnetic and Lattice Fluctuations in Iron Pnictide Superconductors, *Phys. Rev. Lett.* **111**, 137001 (2013).
- [28] K. M. Leung and D. L. Huber, Low-frequency dynamics in cooperative Jahn-Teller systems, *Phys. Rev. B* **19**, 5483 (1979).
- [29] J. H. Page and S. R. P. Smith, Microwave ultrasonic attenuation above the Jahn-Teller phase transition in TmVO_4 , *J. Phys. C: Solid State Phys.* **16**, 309 (1983).
- [30] F. Borsa, M. Corti, and A. Rigamonti, Electronic spin-dynamics at a structural phase transition by cooperative Jahn-Teller effect: An Al^{27} NMR study in PrAlO_3 , *J. Appl. Phys.* **49**, 1383 (1978).
- [31] M. Corti, A. Rigamonti, and A. Magistris, ^{133}Cs quadrupole perturbed NMR study of Jahn-Teller phase transitions in CsCuCl_3 , *Phys. Status Solidi B* **108**, 29 (1981).
- [32] A. Rigamonti, NMR-NQR studies of structural phase transitions, *Adv. Phys.* **33**, 115 (1984).
- [33] A. Smerald and N. Shannon, Angle-resolved NMR: Quantitative theory of ^{75}As T_1 relaxation rate in BaFe_2As_2 , *Phys. Rev. B* **84**, 184437 (2011).